J Mater Sci: Mater Med
DOI 10.1007/s10856-013-5074-3

A comparative study of zirconium and titanium implants in rat: osseointegration and bone material quality

Rebecca M. Hoerth · María R. Katunar · Andrea Gomez Sanchez · Juan C. Orellano · Silvia M. Ceré · Wolfgang Wagermaier · Josefina Ballarre

Received: 31 May 2013 / Accepted: 12 October 2013

Abstract Permanent metal implants are widely used in human medical treatments and orthopedics, for example as hip joint replacements. They are commonly made of titanium alloys and beyond the optimization of this established material, it is also essential to explore alternative implant materials in view of improved osseointegration. The aim of our study was to characterize the implant performance of zirconium in comparison to titanium implants. Zirconium implants have been characterized in a previous study concerning material properties and surface characteristics in vitro, such as oxide layer thickness and surface roughness. In the present study, we compare bone material quality around zirconium and titanium implants in terms of osseointegration and therefore characterized bone material properties in a rat model using a multi-method approach. We used light and electron microscopy, micro Raman spectroscopy, micro X-ray fluorescence and X-ray scattering techniques to investigate the osseointegration in terms of compositional and structural properties of the newly formed bone. Regarding the mineralization level, the mineral composition, and the alignment and order of the mineral particles, our results show that the maturity of the newly formed bone after 8 weeks of implantation is already very high. In conclusion, the bone material quality obtained for zirconium implants is at least as good as for titanium. It seems that the zirconium implants can be a good candidate for using as permanent metal prosthesis for orthopedic treatments.

Electronic supplementary material The online version of this article (doi:10.1007/s10856-013-5074-3) contains supplementary material, which is available to authorized users.

R. M. Hoerth · W. Wagermaier
Department of Biomaterials, Max Planck Institute of Colloids and Interfaces, 14424 Potsdam, Germany
e-mail: rebecca.hoerth@mpikg.mpg.de

R. M. Hoerth
Berlin-Brandenburg School of Regenerative Therapies (BSRT) at Charité Campus Virchow-Klinikum, 13353 Berlin, Germany

M. R. Katunar · A. Gomez Sanchez · S. M. Ceré · J. Ballarre (✉)
INTEMA - CONICET - Universidad Nacional de Mar del Plata, Juan B. Justo 4302, B7608FDQ Mar del Plata, Buenos Aires, Argentina
e-mail: jballarre@fi.mdp.edu.ar

J. C. Orellano
Traumatología y Ortopedia, Hospital Interzonal General de Agudos "Oscar Alende", Mar del Plata, Argentina

1 Introduction

Metal prostheses are widely used in human medical applications and in orthopedics, for example permanent titanium alloy implants such as hip joint replacements. They are supposed to rest for several tenths of years within the patient's body and to bear the load, the former joints carried. Therefore, it is not only important to further investigate and enhance implant materials and ways of processing but also to continuously look for new possibilities concerning the implant materials or investigate other methods.

Generally, metal implants for example made of titanium or zirconium have excellent mechanical properties in relation to their size and their weight, as discussed in detail for titanium by Navarro et al. [1]. However, metal implants always bear a risk of corrosion and of ions, migrating into the surrounding tissues [2, 3]. Many studies have been performed to improve the corrosion behavior of permanent metal implants, such as stainless steel implants, using for

Published online: 30 October 2013

example coatings to protect the metal from the surrounding media [2–5]. By applying double layer coatings consisting of an inner titanium layer and an outer hydroxyapatite layer, corrosion resistance as well as bioactivity and osseointegration of dental endodontic implants can be improved [5]. But also titanium, being bioinert, profits from additional coatings to enhance new bone formation, as shown in in vivo and in vitro studies [6]. Hence, coatings might enhance the corrosion resistance, but also the implant's bioactivity and improve bone formation and implant integration [7–9].

In general, there is a wide range of possible materials used in orthopedics. Titanium and some of its alloys are nowadays the most common materials for permanent prosthesis, as they are corrosion resistant, show osseointegration, have a moderate elastic modulus and a relatively low density [1]. It can be surface treated to become more bioactive (e. g. by hydroxyapatite plasma spray surface treatment) but titanium is also relatively difficult to handle and hard to process [1]. A material with comparable properties related to implant performance is zirconium [10, 11]. In fact, zirconia (ceramic ZrO_2) is a well-established material in dental implant technology, but the metal zirconium is not yet tested intensively in view of its potential as implant material. It has slightly different mechanical properties compared to titanium, for example a lower hardness and a lower Young's modulus. The hardness could be increased by reducing the grain size to obtain ultrafine grained zirconium with values similar to those of titanium alloys [11]. Compared to pure titanium, a lower Young's modulus could reduce stress shielding [12]. Thus, zirconium with its lower stiffness might even enhance the implant integration by decreasing stress shielding. Both metals naturally form an oxide layer and are therefore known to be bioinert [1, 13]. In previous work, the surface modification by anodizing treatment and the resulting surface characteristics of commercially pure zirconium and titanium were analyzed in detail [14–16]. In these previous studies, the thickness of the artificially formed oxide layer and the surface roughness increased with the potential during the anodizing treatment. The phosphorous content within the oxide layer was supposed to increase due to anodizing in H_3PO_4 solution [14, 16]. Furthermore, it was found for zirconium implants, that the barrier effect and the rupture potential were optimized for an anodizing process with a potential of 30 V [15]. As the chemical, compositional and structural changes of the surface are supposed to improve the bioactivity of implants and the osseointegration we decided to do further studies with this alternative to the established titanium implants.

In this paper, we study the implant performance in an animal model and our aim is to investigate the osseointegration of zirconium and the resulting bone material quality. Based on our hypothesis that zirconium could be a possible alternative to the established implant material titanium we describe the material structure of the newly grown bone around zirconium implants and compare our results with those of titanium implants. We apply a multi-method approach to characterize the bone material at different length scales, using light, cross polarized light and electron microscopy, Raman spectroscopy, X-ray fluorescence, and small angle X-ray scattering techniques, to analyze quality, maturity, and structure of the integrating bone. Therefore we investigate needle-shaped titanium and zirconium implants within a rat model, where the implants are introduced within the marrow cavity, as descried in [17]. To enhance the effects of the oxide layer, we studied an anodizing treatment, leading to an artificially produced, thicker oxide layer.

2 Materials and methods

2.1 Implant processing

Commercially pure zirconium (702, 99.5 %, Roberto Cordes S.A., Argentina, impurities: C 90 ppm max, Fe + Cr 700 ppm max, H 3 ppm max, Hf 70 ppm max, N 30 ppm, O 900 ppm max) and titanium (grad 2, 99.3 %, Robert Cordes S.A., Argentina, impurities: C 1000 ppm max, Fe 3000 ppm max, H 100 ppm max, N 300 ppm max, O 2500 ppm max) cylinders were used to produce needle-shaped metal implants with a diameter of 0.8 mm (Zr) and 1 mm (Ti) and a length of 20 mm. After cleaning with acetone the implants were dried and stored in a desiccator. An artificial oxide layer was produced using an anodic polarization treatment as described before in several studies [9, 18]. In this system, the metal implant served as working electrode and a stainless steel mesh as counter electrode within a two-electrode cell. They were anodized in 1 mol/l H_3PO_4 solution at 30 V during 3600 s, as already suggested in [15, 16]. The different groups of implants are explained in Table 1.

2.2 Surgical implantation and sample preparation

Eight Wistar rats (male, 10 week old, weight between 300 g and 400 g) were used to perform the experiments. In four animals we implanted titanium and in another four animals zirconium samples. In each animal, one leg has a control implant (without anodizing treatment) and the other leg an anodized implant (see Table 1). It was taken care of surgical procedures, analgesia, standards of living and appropriated death as demands the Mar del Plata National Hospital's Interdisciplinary Ethics Committee (HIEMI and HIGA Mar del Plata National Hospital's, approbation April 2009) and in

accordance to the Animal Welfare Act and the NIH Guide for care and use of laboratory animals. The rats were anesthetized with fentanyl citrate and droperidol (4 ml/kg according to their weight, Janssen Lab, Johnson and Johnson). After sterilization in an autoclave, the implants were placed into the rat long bones by press fit [17, 19]. Radiographs were taken in order to control the correct position of the implants within the medullary canal. After 8 weeks the animals were sacrificed with an overdose of intraperitoneal fentanyl citrate and droperidol (acting as a neuroleptanalgesic). The bones were explanted and cleaned from surrounding tissue. After fixation in neutral 10 wt% formaldehyde during 1 day and dehydration in increasing series of ethanol solutions the samples were embedded in polymethyl methacrylate (PMMA). The implantation and sample retrieving procedure was described earlier in more details [17, 19].

The samples were then cut into cross-sections to investigate the bone material at the interface between the implant and the marrow or the cortical bone, using a low speed diamond saw (Isomet Low Speed Saw, Buehler, USA) cooled with water. If thinner samples were required for the methods, the sections were ground with grid paper. Altogether, eight different kinds of sample cross-sections were analyzed: one non-treated and one 30 V anodized titanium implant and also one non-treated and one 30 V anodized zirconium implant (named Ti0, Ti30, Zr0, and Zr30), each of them cut into four slices in the midshaft region and four slices within the epiphysis (see Table 1). In general, as already suggested in [19], three different regions of interest were investigated, the newly formed bone around the implant, where the implant was originally in contact to the bone marrow (referred to as marrow zone, abbreviated by M), or in contact to the cortical bone (remodelation zone, R) and the cortical bone itself (C) to obtain reference values for comparison (see Fig. 1). To analyze the quality of the newly formed bone deposited at the implant surface we used a multi method approach as described below. The different characterizing methods can be seen in Table 1.

2.3 Light and electron microscopy

Light and electron microscopy images were both taken on one set of eight samples using standardized methods and were performed for precharacterization reasons to prepare the subsequent measurements. Figure 1 shows two Zirconium samples (30 V anodized and unanodized) at the same section height (within the midshaft). Sample cross-sections with a thickness of about 130 μm were observed with an optical light microscope (LM) and afterwards analyzed using cross polarized light (PLM) (Leica DM RXA2, Wetzlar, Germany). Histological sections were stained with toluidine blue staining solution (0.01 g/ml, Cicarelli, Argentina) and characterized using an LM (Olympus BH2 Microscope, Japan). Scanning electron microscopies (SEM) were made using an environmental scanning electron microscopy (SEM, FEI-Company, Oregon, USA) in back-scattered electron mode (BSE). The images were performed at an acceleration voltage of 10 kV at working distances of about 12.5 mm in low vacuum mode (pressure 0.75 Torr) with a magnification of 100.

2.4 Micro X-ray fluorescence (XRF)

XRF measurements were performed at the D09B XRF Fluorescence beamline of the Brazilian Synchrotron Light Laboratory (LNLS, Campinas-SP), see also [20], using a white beam excitation and an energy dispersive Si(Li) detector (Canberra Industries, Inc.) (energy resolution of 165 eV at 5.9 keV). The X-ray beam was 20 μm in diameter and was generated by a fine conical monocapillary. For the experiment, the samples (slides of 150 μm thickness) were glued on a Kapton tape and mounted on a sample holder. The standard excitation-detection geometry (45° + 45°) was used. A filter (two aluminum foils, 30 μm thick) placed at the detector entrance was used in order to reduce the strong intensity of the calcium fluorescence peak coming from the samples. XRF maps of about 16 × 16 points (step sizes of 25 μm in x- and 20 μm in

Table 1 Quantity of samples per metal and surface treatment

Metal	Surface treatment	Cross-section position
Titanium (four rats)	Untreated (four samples)	Midshaft (several cuts)
		Epiphysis (several cuts)
	30 V anodized (four samples)	Midshaft (several cuts)
		Epiphysis (several cuts)
Zirconium (four rats)	Untreated (four samples)	Midshaft (several cuts)
		Epiphysis (several cuts)
	30 V anodized (four samples)	Midshaft (several cuts)
		Epiphysis (several cuts)

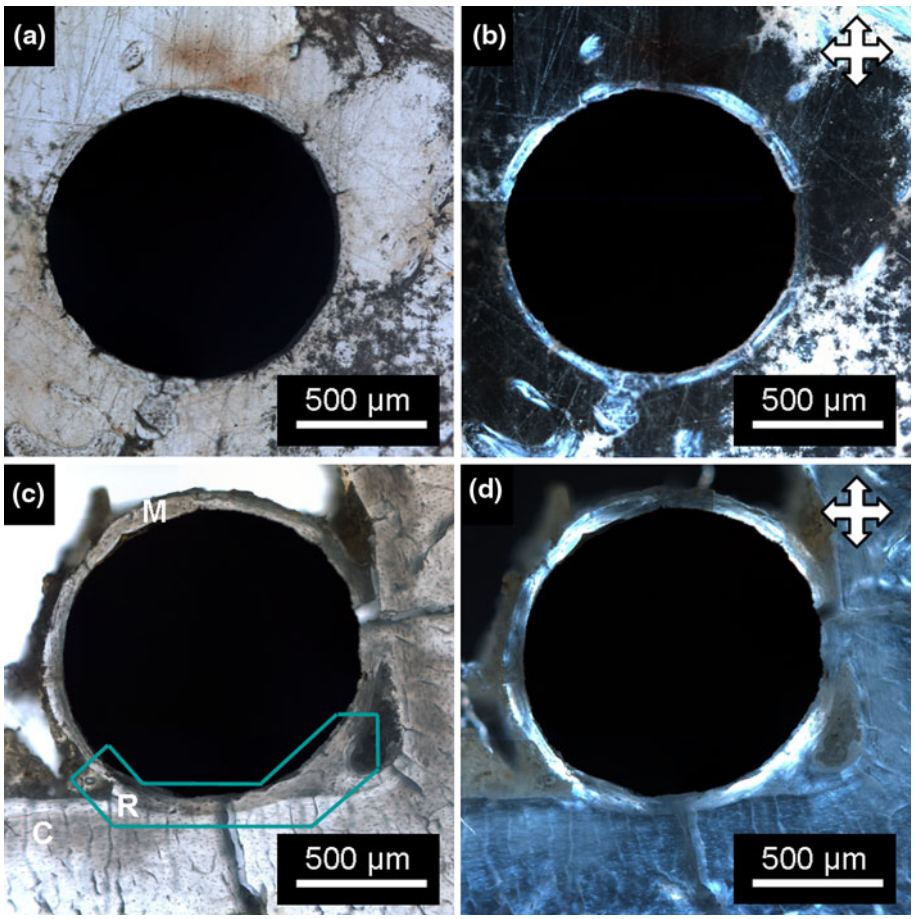

Fig. 1 Light and cross polarized light microscopies of the samples Zr0 (**a**, **b**) and Zr30 (**c**, **d**) to get a first overview of the bone ingrowths and to visualize the circumferential orientation of the collagen matrix. **c** Different regions of interest are illustrated (M: marrow zone, R (*blue box*): remodelation zone and C: cortex) (Color figure online)

y-direction) showing the implant and the surrounding tissue (newly formed bone, marrow, and cortex), were measured. The collecting time was fixed to 15 s per point having an average detector deadtime of around 10 %. Measurements of additional XRF spectra in single points within the cortex were taken during 100 s. The PyMCA (Phyton multi-channel analyzer) program [21] was used for spectrum fitting and also for correcting the attenuation of the fluorescence signal due to the aluminum filter. We mainly concentrated on the calcium content as well as on the titanium and the zirconium XRF signal.

2.5 Micro Raman spectroscopy

Cross-sections of about 200 µm thickness were superficially cleaned with isopropyl alcohol and then used to do Micro Raman spectroscopy. The experiments were performed using a Renishaw in Via Reflex (Renishaw, England) spectrometer. To record the spectra, it was coupled with a CCD detector (1040 × 256 pixels) and Leica microscope (DM2000, Leica, Germany) and we used a 50 × Leica microscope objective (0.75 NA). The obtained spectral resolution was 4 cm^{-1}. The system was working with a 785 nm laser diode as excitation source, combined with a grating of 1200 grooves/mm. To avoid sample damages, we kept the laser power below 10 %. The acquisition time was 30 s per measurement point. First, several line scans of 200 µm (20 points) were performed going from the marrow or the cortex through the newly formed bone until the implant (example shown in Fig. 4). For statistical analysis, additional meshes of 4 × 5 points were measured in three regions of interest (marrow zone, remodelation zone, and cortex). The background was subtracted using a modified polynomial fitting algorithm. With a custom-developed Matlab program (Dr. Adrian Cisilino (2011), Matlab, Mathworks), the amide I (1650 cm^{-1}), the amide III (1245 cm^{-1}), the β-carbonate (1071 cm^{-1}), the ν_1 phosphate (960 cm^{-1}), and the ν_2 phosphate (430 cm^{-1}) peak intensities were recorded. Two different mineral to matrix ratios (ν_1 PO_4^{3-}/amide I and ν_2 PO_4^{3-}/amide III) as well as the degree of carbonate substitution within the apatite lattice (CO_3^{2-}/ν_2 PO_4^{3-}) and the degree of crystallinity ($FWHM^{-1}$ of ν_1 PO_4^{3-}) were calculated. Afterwards, the results of each mesh were averaged and statistically analyzed (values are given in Table 2).

Table 2 Mineral to matrix ratios, degree of carbonate substitution, and crystallinity values calculated based on Raman measurements using 20 measurement points for each value

	Mineral to matrix ratio I ν_1 PO_4^{3-}/amide I	Mineral to matrix ratio II ν_2 PO_4^{3-}/amide III	Carbonate Substitution CO_3^{2-}/ν_2 PO_4^{3-}	Crystallinity FWHM^{-1}of ν_1 PO_4^{3-}
Ti0				
R	9.27 ± 0.66	1.78 ± 0.15	1.13 ± 0.04	0.0521 ± 0.0006
M	7.66 ± 0.15	1.81 ± 0.10	1.12 ± 0.06	0.0534 ± 0.0004
C	9.04 ± 0.28	1.93 ± 0.15	1.08 ± 0.03	0.0532 ± 0.0003
Ti30				
R	7.53 ± 0.21	2.15 ± 0.13	0.90 ± 0.07	0.0553 ± 0.0004
M	7.29 ± 0.22	1.95 ± 0.12	0.89 ± 0.10	0.0558 ± 0.0004
C	11.11 ± 0.38	2.22 ± 0.07	1.19 ± 0.06	0.0558 ± 0.0003
Zr0				
R	8.31 ± 0.23	2.04 ± 0.18	0.86 ± 0.06	0.0540 ± 0.0004
M	9.81 ± 0.39	2.64 ± 0.18	0.84 ± 0.10	0.0531 ± 0.0006
C	9.07 ± 0.40	1.82 ± 0.14	1.17 ± 0.04	0.0553 ± 0.0007
Zr30				
R	8.26 ± 0.37	2.32 ± 0.17	1.04 ± 0.05	0.0544 ± 0.0004
M	6.89 ± 0.46	2.69 ± 0.20	1.05 ± 0.07	0.0536 ± 0.0004
C	8.65 ± 0.25	2.01 ± 0.06	1.21 ± 0.03	0.0567 ± 0.0004

Values are given for every condition (Ti0, Ti30, Zr0, and Zr30) and all the defined regions of interest (R, M, and C) as mean ± SD

2.6 Small angle X-ray scattering (SAXS)

The samples for the laboratory X-ray equipment (about 200 μm thick) were fixed on a holder, perpendicular to the X-ray beam path. The SAXS measurement points were specified using an X-ray radiograph and selected in order to be within the newly formed bone around the metal implant (marrow and remodelation zone) and in the cortex. Thereby about 25–40 measurement points were chosen within the area around the implants (marrow and remodelation zone). The X-ray beam with a wavelength of 1.5418 Å was generated by an X-ray generator (Bruker, AXS, Karlsruhe, Germany) with a rotating copper anode operating at 40 kV and 100 mA (Cu Kα radiation). It was collimated by a setup system with two pinholes and had a diameter of 200 μm in the focus. The sample-to-detector distance was about 600 mm and the calculation of the beam center and the exact distance was done using a silver behenate standard. The scattering signal was acquired during 3600 s per measurement point and recorded by a position sensitive area detector (HI-STAR, Bruker AXS, Karlsruhe, Germany, pixel size 105.26 × 105.26 μm^2).

Two sections of the non-treated zirconium sample (midshaft and epiphysis) were investigated at the μSpot beamline of the synchrotron radiation source BESSY II (Berliner Elektronenspeicherring-Gesellschaft für Synchrotronstrahlung, Helmholtz-Zentrum Berlin, Germany). Therefore, samples were ground to a thickness of about 50 μm and mounted on a sample stage in order to move it in x- and y-direction, perpendicular to the X-ray beam path at a sample-to-detector distance of about 400 mm. A quartz standard was used for calibration. The calcium XRF signal helped to detect the bony tissue around the metal implant and to determine the measurement points. The points were chosen to be in the small layer of newly formed bone around the implant (only marrow zone) with a distance of 30 μm one from the other. Scattering measurements then were performed with an X-ray beam with a beam size of 10 μm, defined by a two pinhole setup, and at a wavelength of 0.82656 Å. The scattering pattern was collected during an exposure time of 48 s with a position sensitive CCD-detector (MarMosaic 225, Mar USA Evanston, USA) (pixel size 73.242 × 73.242 μm^2). Afterwards the scattering results were corrected regarding the decreasing ring current and the intensity variations.

Analysis of both X-ray scattering experiments were performed using AutoFit (custom-made Fit2D-based software by Max Planck Institute of Colloids and Interfaces, Potsdam, Germany). Several parameters giving the orientation and the size of the mineral particles within the bone tissue were determined as described in [22].

3 Results

Several methods were used to investigate different samples aiming to compare bone formation, resulting bone quality and implant integration around titanium and zirconium implants.

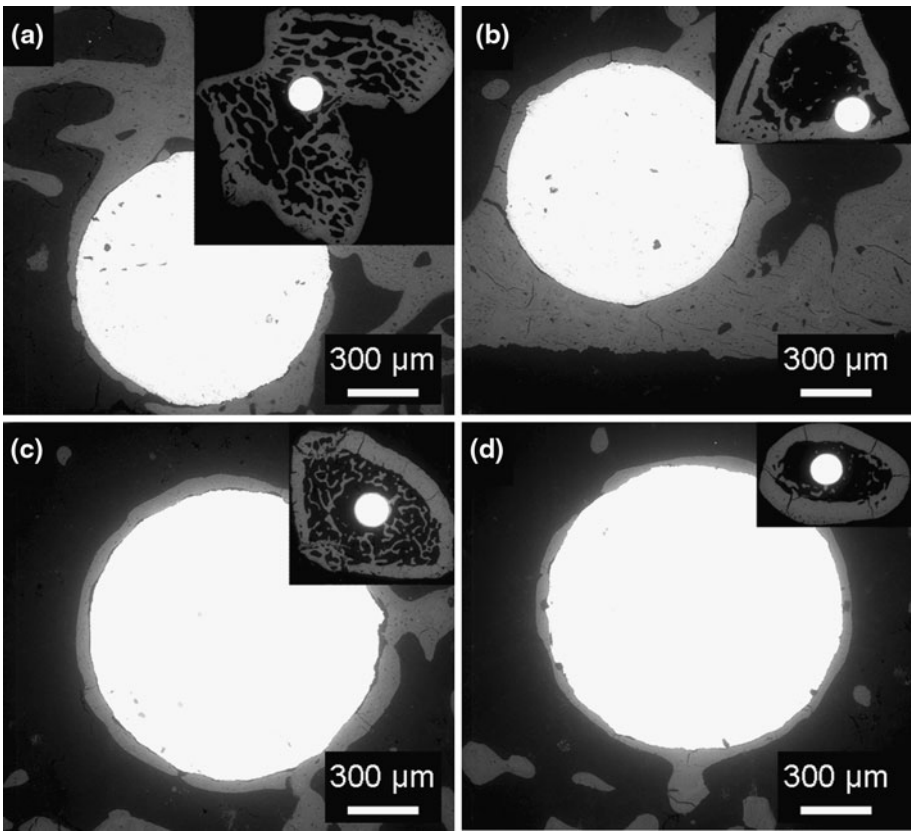

Fig. 2 BSE images of Ti0 (**a**, **b**) and Zr0 (**c**, **d**) within the epiphysis (**a**, **c**) and in the midshaft region (**b**, **d**). The *insets* show the whole cross-section whereas the main pictures give qualitative impressions of the mineral content of the newly formed bone

3.1 Light and electron microscopy

Light microscopies show a small continuous bone layer around the metal implants and give a first overview of the bone formation around the implant (Fig. 1, sample Zr0 and Zr30, in the midshaft region). For all the samples, the implant is well integrated. Using cross polarized light, the same areas can be analyzed regarding the orientation of the organic collagen matrix, showing a highly ordered structure, where the collagen fibrils are oriented circumferentially to the implant surface. Comparing the different samples, regarding the integration and the matrix orientation of the newly grown bone, no differences between the two metals and the different surface treatments can be observed. Toluidine blue stained sample sections, studied using light microscopy, visualize again the newly formed layer of bone around the implant, the lamellar ordered structure of the newly formed bone and the osteocytes within the bone and they are used as characterizations for following experiments.

Figure 2 shows SEM images in BSE mode of the samples Ti0 and Zr0, both within the epiphysis and in the midshaft region. The BSE signal is more intense if the nucleus of the atom is larger. So, the white area in the middle of each image is the metallic implant. As Ca is the largest atom present in bone material, BSE imaging can serve to qualitatively analyze the calcium content of the bone, where brighter grey level signify higher amounts of Ca. This detection mode and the evaluation of the different grey scales have been described previously in [23]. Regarding this, we can say, that the mineralization within the newly formed bone is within the range of the cortical bone for all the four conditions (Ti0, Ti30, Zr0, and Zr30, in the midshaft region as well as in the epiphysis).

3.2 Micro XRF

We use XRF mapping to investigate the mass fraction of Ca and of the corresponding implant metal (Ti or Zr) present in the newly formed bone, in the surrounding marrow and in the cortex. Figure 3 demonstrates for the samples Ti30 and Zr0 that the Ca mass fraction (Fig. 3b, d) in the newly formed bone is within the range of the cortical bone, so we can confirm again, that the mineralization is similar to the existing cortex. Only at the interface right next to the implant, a slight decrease of Ca can be detected. More important is the fact that the concentration of migrating metal ions from the implant into the tissue is negligible. Figure 3a, c show the Ti and the Zr mass fractions within the samples (same areas as in Fig. 3b, d). For each image the implant is at the right side, surrounded

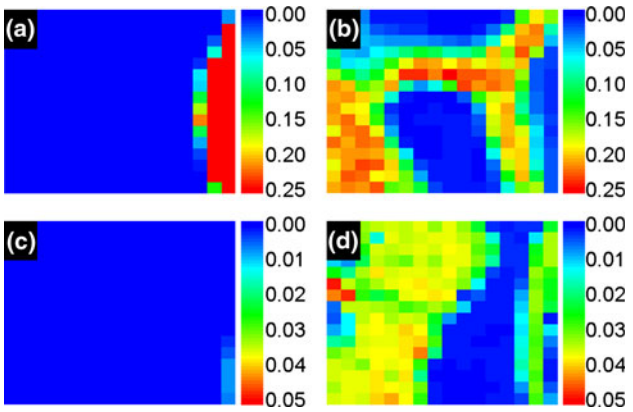

Fig. 3 XRF map measurement showing the metal (Ti in **a** Zr in **c**) and the Ca mass fraction (**b**, **d**) within the area around the implants of midshaft cross-sections of the Ti30 (**a**, **b**) and the Zr0 sample (**c**, **d**)

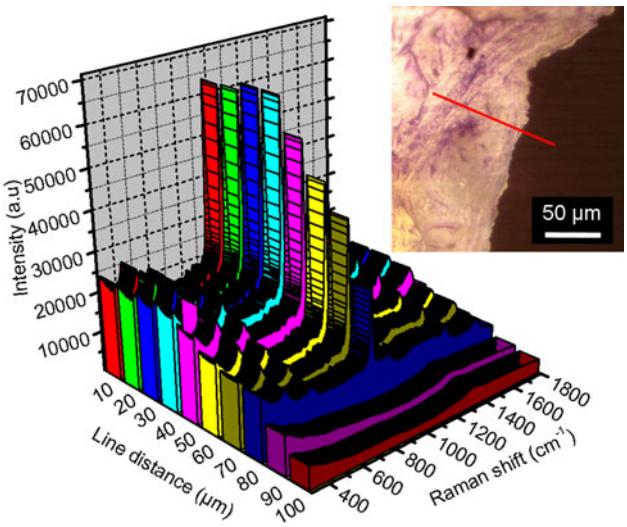

Fig. 4 Line scan of a Raman spectroscopy measurement of sample Zr30. The *red line* shown in the *inset* corresponds to the line distance shown in the main image, reaching from the cortex to the implant (Color figure online)

by the newly formed bone layer. The values can only give a qualitative statement but averaging the ten highest Ti values of Fig. 3a gives a mass fraction of 0.537 (with top values of around 0.6) for the points measured within the implant. Assuming that this corresponds to the metal implant, we can say, that the values in the surrounding tissue (all color-coded in dark blue) are very low. For the Zr0 measurement, we only scratched the implant so we cannot give a value for the implant area but still the Zr content of the surrounding tissue is obviously very low.

3.3 Micro Raman spectroscopy

Figure 4 illustrates a micro Raman analysis of the interface between an anodized zirconium implant (Zr30) and the newly formed tissue by a line scan. In total, 20 points were measured along a line starting from the old bone, crossing the newly formed bone and the interface between implant and bone, and finishing in the implant. In Fig. 4, micro Raman spectra of ten points are shown and the inset shows a microscopy of the toluidine blue stained section of the considered area. The red line specifies the corresponding measurement line. The spectra indicate the decrease in the intensity of the ν_1 PO_4^{3-} peak at 960 cm^{-1} while leaving behind the cortex and going to the remodelation zone and its vanishing when we arrive in the metal implant. The most significant peaks of the bone tissue spectra are the ν_1 PO_4^{3-} (960 cm^{-1}) and the ν_2 PO_4^{3-} (430 cm^{-1}), both representing the phosphate binding vibrations, the CO_3^{2-} peak (1071 cm^{-1}), showing β-carbonate bindings, the amide I (1650 cm^{-1}) and the amide III peak (1245 cm^{-1}), standing for the collagen, representing the organic part of the bone tissue. Using all these results we calculated two mineral to matrix ratios (ν_1 PO_4^{3-}/amide I and ν_2 PO_4^{3-}/amide III) to describe the chemical composition of the bone material. As the ν_1 PO_4^{3-} and the amide I bands depend on the structured orientation (collagen fibrils) [24], we mainly analyzed the ratio II (ν_2 PO_4^{3-}/amide III) for our discussion. For further descriptions of the mineral composition we also calculated the crystallinity ($FWHM^{-1}$ of ν_1 PO_4^{3-}) [25] and the carbonate substitution (CO_3^{2-}/ν_2 PO_4^{3-}) within the lattice [26]. The calculations were done for two animals per condition, always in the midshaft region, but as the results for the different animals were comparable, and we have to take into account the biological variability, we give here only the statistically analyzed values for one animal of each condition (Table 2).

Regarding the mineral to matrix ratio II, the values for the titanium samples are slightly lower for the marrow and the remodelation zone compared to the cortex signifying a lower degree of mineralization and higher collagen content. In contrast, the zirconium samples show high values for the remodelation zone and even higher values for the marrow (Zr0: marrow 2.64, remodelation zone 2.04, and cortex 1.82, Zr30: 2.69, 2.32, and 2.01, respectively). So for the zirconium implants, we can see that the degree of mineralization of the new bone around the implant is even higher than in the cortex and that we have a large deposition of hydroxyapatite within the organic matrix.

Considering the carbonate substitution, lower values signify a lower degree of substitution and therefore a younger tissue [27]. We have similar values for the different regions of interest for the untreated titanium sample but considerably lower values in the newly formed bone for the treated titanium sample and the two zirconium samples. So remembering the high mineralization values that we got for the zirconium samples from the mineral to matrix ratio we still have to state, that the newly formed bone is still

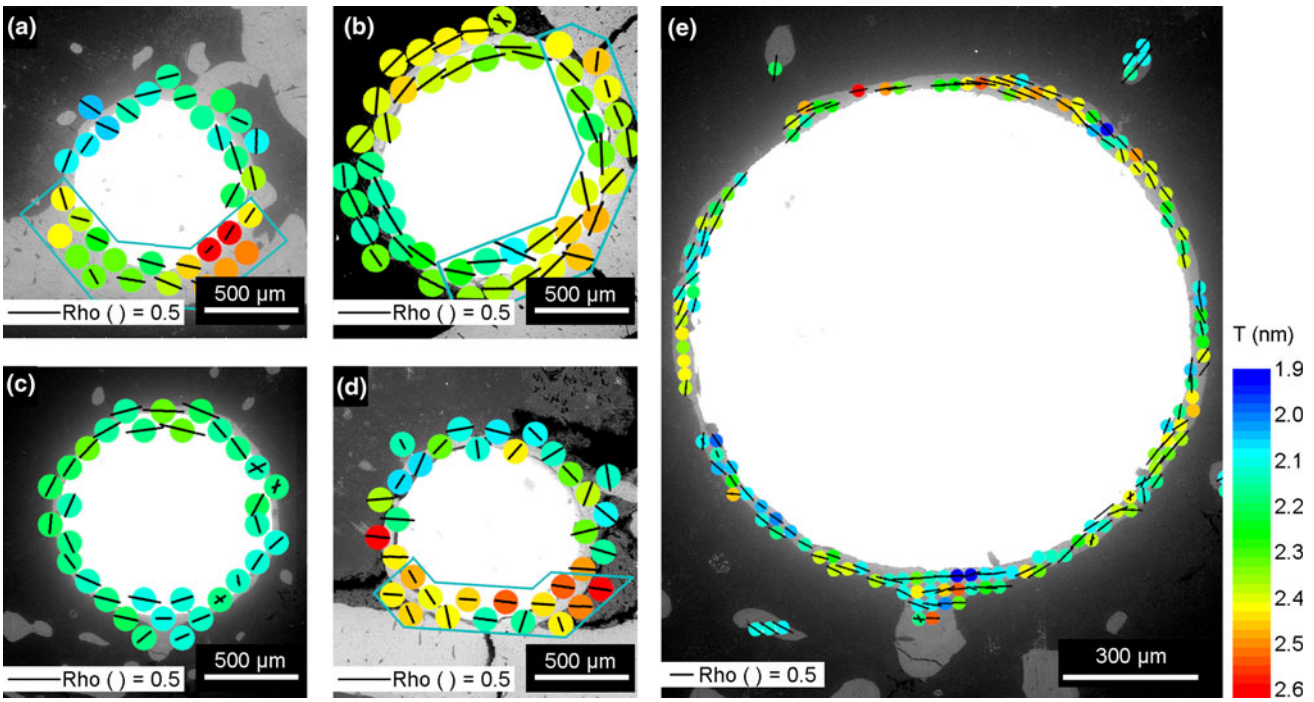

Fig. 5 **a–d** The results of the SAXS experiments for the samples Ti0, Ti30, Zr0, and Zr30 in the midshaft region, measured with the laboratory X-ray source. **e** The sample Zr0 measured at the synchrotron radiation source BESSY II. The T parameter (thickness of particles) is given *color-coded* the rho parameter (degree of orientation) by the *length* of *black bars* and the orientation by the *orientation* of the *bars*. The *box* marks the measurement points within the remodelation zone, the others are the points within the marrow zone (Color figure online)

young and has less substituted β-carbonates. Even highly mineralized, the lattice is not yet as much transformed as in the cortex. As a last parameter we considered the crystallinity and here the values for all the four conditions are similar in the three different regions.

3.4 SAXS

The two dimensional SAXS images were integrated either radially to calculate the averaged mineral thickness (defined as the T parameter) or azimuthally to obtain the degree of alignment (rho parameter) and the preferential orientation of the mineral particles [22]. With scanning SAXS measurements, the newly formed bone around the implant was analyzed and compared to the cortical bone as a reference. Figure 5 shows BSE images of the four conditions (Fig. 5a–d shows the samples Ti0, Ti30, Zr0, and Zr30 and Fig. 5e shows again sample Zr0 in higher resolution) in the midshaft region. The SAXS results are given by a color-coding representing the calculated T parameters and the small black bars give the arrangement of the mineral particles in the measured spots of the newly formed bone. The length of the bars denotes the degree of alignment of the particles (rho parameter, where rho = 1 means fully aligned) and the direction of the bars give the overall preferred orientation of the mineral particles. These SAXS results are shown in Fig. 5 laid over the mentioned BSE images. In addition to the measurements at the X-ray source in the laboratory, the sample Zr0 was also analyzed at the synchrotron radiation source with a higher resolution, shown in Fig. 5e. It can be seen that the alignment of the rho bars is circumferential to the implant, especially in the case of the zirconium samples. The orientation seems more randomized when the material is titanium, either with or without the surface treatment. This circumferential orientation confirms the expectations, that we had considering the polarized light microscopies, where we stated a circumferential orientation of the collagen fibrils. Now we see that the mineral platelet orientation goes along with the orientation of the collagen matrix.

For the analysis, we distinguished between the different regions of interest, following the separation into cortex, marrow zone and remodelation zone in [19]. The measurement points, considered to belong to the remodelation zone are surrounded by a blue box, the other points belong to the marrow zone, and the reference points (cortex) are not shown in Fig. 5. Regarding this, the T parameter values for the marrow zone are slightly lower than the values for the remodelation zone (Table 3). In the Zr0 sample (Fig. 5c, e) we only have marrow zone and no remodelation zone as here the implant was introduced into a femur, not touching the cortex (the other samples are tibia

Table 3 Rho and T values, resulting from SAXS experiments, done for every condition (Ti0, Ti30, Zr0, and Zr30) and for the regions of interest (R, M, and C) both in the midshaft region and within the epiphysis

	rho (mean ± SD)	T (nm) (mean ± SD)
Ti0		
Midshaft		
R	0.22 ± 0.07	2.40 ± 0.13
M	0.24 ± 0.04	2.15 ± 0.09
C	0.24 ± 0.09	2.49 ± 0.02
Epiphysis		
M	0.25 ± 0.06	2.08 ± 0.13
C	0.19 ± 0.00	2.11 ± 0.11
Ti30		
Midshaft		
R	0.20 ± 0.04	2.36 ± 0.18
M	0.27 ± 0.05	2.26 ± 0.18
C	0.19 ± 0.06	2.37 ± 0.14
Epiphysis		
M	0.25 ± 0.11	2.12 ± 0.07
C	0.27 ± 0.05	2.28 ± 0.06
Zr0		
Midshaft (laboratory)		
M	0.24 ± 0.08	2.19 ± 0.04
C	0.22 ± 0.09	2.40 ± 0.09
Midshaft (synchrotron)		
M	0.40 ± 0.11	2.24 ± 0.16
Epiphysis (laboratory)		
M	0.23 ± 0.08	2.27 ± 0.07
C	0.22 ± 0.07	2.36 ± 0.22
Epiphysis (synchrotron)		
M	0.36 ± 0.11	2.31 ± 0.20
Zr30		
Midshaft		
R	0.29 ± 0.07	2.36 ± 0.09
M	0.30 ± 0.05	2.30 ± 0.09
C	0.23 ± 0.09	2.40 ± 0.04
Epiphysis		
M	0.22 ± 0.07	2.26 ± 0.10
C	0.17 ± 0.03	2.32 ± 0.16

For the Zr0 sample additional measurements were performed at the synchrotron radiation source BESSY II. As the Zr0 sample was introduced into the tibia (the others into the femur) we did not get values for the remodelation zone

implants). The same SAXS experiments have also been performed for cross-sections in the epiphysis (see Supplementary Figure). Regarding this figure, the T parameters for the titanium samples are lower than the values for the zirconium samples. All the points can be considered as marrow zone, as the implant does not touch the cortex and compared to the values of the midshaft region they also resemble rather the values of the marrow zone. Table 3 gives the calculated values of the T parameter in nm and the Rho parameter of the Ti0, Ti30, Zr0, and Zr30 implants. The values are given for the different regions of interest (R corresponds to the measurement points within the blue boxes in Fig. 5, M to the other points and C to the reference points in the cortex). The T parameter values of the remodelation zone are in the same range as at the reference for all studied cases and slightly lower within the marrow zone (e.g. Ti30: marrow 2.26, remodelation zone 2.36, and cortex 2.37, Zr30: 2.3, 2.36, and 2.4, respectively). Lower T parameter values denote thinner mineral crystals within the tissue. For the untreated zirconium implant (Zr0) the calculated values for both, the measurements at the laboratory X-ray source and the measurements at the synchrotron radiation facility BESSY II are given. The T parameter values are nearly the same, for both, in the midshaft region and in the epiphysis (Zr0, midshaft; 2.19 with the laboratory source and 2.24 with the synchrotron radiation source). For the rho parameters differences between the different regions of interest for all the four cases are not significant (see Table 3), in the midshaft as well as in the epiphysis. However, the rho parameters measured at the laboratory source are smaller than the one measured at the synchrotron radiation source (Zr0, midshaft: 0.24 with the laboratory source and 0.40 with the synchrotron radiation source, epiphysis: 0.23 and 0.36, respectively). Because of the smaller beam size (10 μm at the synchrotron source BESSY II and 200 μm in the laboratory) and the thinner sample sections (around 50 μm for the synchrotron experiment at BESSY II and 200 μm for the laboratory X-ray source) a much higher resolution was achieved and so a smaller sample volume was irradiated, taking into account only fewer mineral particles. The calculated direction of the predominant orientation and the amount of orientated particles is more precise so that it can be assumed that the values for the other samples would also be higher than calculated for the experiments in the laboratory. This means that the newly formed bone is already relatively good oriented.

4 Discussion

Our results lead us to the proposition that zirconium implants get surrounded by a dense and compact layer of new bone, and that they show very good osseointegration behavior. The results obtained for zirconium samples compared to titanium are at least equal, regarding the quality and the compositional and structural properties of the bone. In our work, we studied a rat model with permanent needle-shaped titanium and zirconium implants

and used a multi-method approach to describe and characterize the structure and the quality of bone tissue formed in the osseointegration process. The combined use of microscopy techniques, micro Raman spectroscopy, micro XRF, and SAXS techniques to investigate the structure and composition of the newly formed bone, give a complete overview of the mineral deposition, maturation, and aging process of bone during implant fixation. We intended to do a first study on zirconium as a possible alternative to titanium and therefore we considered the small number of animals as appropriate. Based on our hypothesis that zirconium implants can be a candidate for using as permanent metal prosthesis for orthopedic treatments we compared the implant performance of zirconium to the results of titanium.

The anodizing treatment was applied to improve the bioactivity of the implants. Already in bare condition, titanium and zirconium are both considered to be bioinert because of their naturally formed oxide layer. The anodic treatment in phosphoric acid enlarges the thickness of the oxide layer from a few nanometers to several hundred nanometers [18]. The surface characteristics of titanium and zirconium, concerning such anodizing treatments, have been investigated previously [14–16] and it was found, that the thickness of the oxide layer increases with increasing potential. Additionally the surface roughness of the anodized samples is bigger and the topography is changed [14, 16]. For the zirconium samples, the rupture potential and the barrier effect of the oxide layer are increased using a potential of 30 V [15]. In summary, the chemical properties and the roughness are changed simultaneously and both, the topography and the composition, are thought to play an important role in the first steps of osseointegration, enhancing the attachment of water and proteins [28–30]. In contrast to this, we did not find significant differences in the bone quality and structure, comparing the untreated and the anodized samples after 60 days of implantation. However, as titanium and zirconium, surface-treated or not, seem to be a good substrate for bone ingrowth and as the anodizing treatment enhances the corrosion properties, as tested in simulated body fluid for zirconium implants in [15], it is worthwhile to continue to anodize the implant surface.

Neither migrated metal ions nor debris were present in the surrounding tissue. This is very important, when metals are used as permanent implant materials [31]. As the implants are supposed to stay within the body for several years and to support loading, it has to be ensured that no metal particles get incorporated into the surroundings. Metallosis caused by abrasive wear is a frequent problem in human implant technique, being hard to treat and often necessitating revision surgeries [32]. We used synchrotron XRF mapping to test the bone and marrow tissue around the implants regarding their titanium and zirconium fluorescence signal, and found no hint for metal ions, and only in traces right at the interface. Especially, we found no difference regarding the two metals and the two different surface treatments. Nevertheless, as the anodizing treatment improves the corrosion behavior and therefore minimizes the risk of ion migration [15], it is worthwhile to maintain the procedure as it can be easily performed.

We found that the newly formed bone has a similar mineralization level as the cortical bone. The mineralization level of bone reflects the mechanical competence of bone [23], but for a definite statement on mechanical behaviour further mechanical investigations would be necessary. The maturity and the age of the tissue can be characterized by size and composition of the mineral particles [22]. We found, that the zirconium samples are slightly higher mineralized. However, the implantation period of 8 weeks did not suffice to get a final state of carbonate substitution compared to the cortex, for both the titanium and the zirconium implants. The thickness of the mineral particles is approximately the same for both materials and both surface treatments, but within the remodelation zone the particle thickness is comparable or slightly lower than the thickness within the cortex. The higher mineral to matrix ratio for the zirconium implants indicates a higher degree of hydroxyapatite deposition within the newly formed bone, compared to the cortical bone. During aging the content of β-carbonates within bone decreases, as they get replaced within the lattice [26, 27]. Even if we can find high mineral deposition levels in the zirconium samples, when we evaluate the carbonate substitution level we see that it is lower in the newly formed bone, compared to the cortex. This leads us to the conclusion, that the bone is well mineralized; however it has not yet been transformed and processed as much as the pre-existing cortical bone, showing the youth of the tissue.

Investigating the micro structure of the bone, both the organic and the mineral part showed a well oriented structure, aligned around the implant, circumferentially to the implant surface. The mineral particles, deposited within the organic matrix, were aligned in the same orientation as the collagen fibrils, circumferentially to the implant surface. Analyzing this micro structure with cross polarized light microscopy and X-ray scattering techniques can reveal information about the way, how the new bone was formed. During normal bone formation and bone healing processes two different types of bone can be seen, which are deposited in two successive waves [33]. Quickly growing woven bone, as a first bone tissue, is later replaced by well-ordered lamellar bone and in an ongoing process further remodeled [34]. However, during our experiments, we did not see any residues of woven bone. This could be explained by the duration of implantation, as already

Guglielmotti et al. [35] showed that woven bone around zirconium implants in rat vanish after about 2 weeks. But it could also mean that the implant even served as a scaffold, enabling a highly ordered way of growing. Similar observations were previously described in a sheep model where large defect healing was enhanced by a porous scaffold. Cipitria et al. showed that the struts of the scaffolds served as surface, where lamellar bone was directly deposited. There was no evidence of woven bone and the newly formed bone was arranged around the struts [36]. Hence we assume that also in our case the bone has grown as lamellar bone right from the beginning, oriented circumferentially to the implant surface.

5 Conclusions

Zirconium, surface-treated or not, is a possible material for permanent implants. As the anodizing treatment enhances the corrosion properties it is worth treating the surface. Regarding the quality of the newly formed bone around zirconium implants, the tested properties are equal or better as those of the titanium implants. After 8 weeks, the bone has already reached a high level of organization in both the mineral and the organic part and the maturity is comparable to the normal cortical bone. This leads us to the conclusion that the bone is immediately deposited as lamellar bone, using the implant as a scaffold instead of being laid down as woven bone and then being remodeled. As a perspective it would be interesting to do further studies investigating different time periods of implantation to better understand the process of implant integration during its different stages. Another interesting question would be to compare our results to studies with aged rats, and to see if the osseointegration and implant fixation process differs for elderly individuals. Finally we can say that our initial hypothesis, that zirconium is a promising alternative to the established implant material titanium is true and that it would be worthwhile to further characterize its qualities regarding implant performance.

Acknowledgments The authors would like to thank C. Li, S. Siegel, I. Zenke, and B. Schonert for technical support, the Max Planck Gesellschaft (MPG), the Deutscher Akademischer Austauschdienst (DAAD), and the Deutsche Forschungsgemeinschaft (DFG) for funding. Contributions were made possible by DFG funding through the Berlin-Brandenburg School for Regenerative Therapies. As well, we would like to thank A. Cisilino, B. Valcarce, M. Valdes (INTEMA, UNMdP), and C. Perez (LNLS), for the grateful help in different areas of this study and the Brazilian Synchrotron Light Laboratory (LNLS). We also want to thank the National Research Council of Argentina (CONICET), the National Agency for Science and Technology Promotion (ANPCyT - PICT 00550 and 0917), and the National University of Mar del Plata (UNMdP - 15/G331) for financial support. We especially want to thank the PROALAR exchange program (DAAD funding together with MINCyT, Argentina) for enabling the exchanges between our institutes.

References

1. Navarro M, Michiardi A, Castaño O, Planell JA. Biomaterials in orthopaedics. J R Soc Interface. 2008;5(27):1137–58. doi:10.1098/rsif 2008.0151.
2. Messaddeq SH, Pulcinelli SH, Santilli CV, Guastaldi AC, Messaddeq Y. Microstructure and corrosion resistance of inorganic-organic (ZrO_2-PMMA) hybrid coating on stainless steel. J Non-Cryst Solids. 1999;247:164–70. doi:10.1016/S0022-3093(99)00058-7.
3. Neumann HG, Beck U, Drawe M, Steinbach J. Multilayer systems for corrosion protection of stainless steel implants. Surf Coat Tech. 1998;98(1–3):1157–61. doi:10.1016/S0257-8972(97)00236-3.
4. Chou TP, Chandrasekaran C, Limmer SJ, Seraji S, Wu Y, Forbess MJ, et al. Organic–inorganic hybrid coatings for corrosion protection. J Non-Cryst Solids. 2001;290(2–3):153–62. doi:10.1016/S0022-3093(01)00818-3.
5. Fathi MH, Moosavi S, Mortazavi V. Novel materials for endodontic implant, in vitro and in vivo tests. Dent Res J. 2003;1(1):36–46.
6. Mehdikhani-Nahrkhalaji M, Fathi MH, Mortazavi V, Mousavi SB, Hashemi-Beni B, Razavi SM. Novel nanocomposite coating for dental implant applications in vitro and in vivo evaluation. J Mater Sci Mater Med. 2012;23(2):485–95.
7. Krupa D, Baszkiewicz J, Sobczak JW, Biliński A, Barcz A. Modifying the properties of titanium surface with the aim of improving its bioactivity and corrosion resistance. J Mater Process Tech. 2003;143:158–63. doi:10.1016/S0924-0136(03)00398-4.
8. Rodríguez HH, Vargas G, Cortés DA. Electrophoretic deposition of bioactive wollastonite and porcelain-wollastonite coatings on 316L stainless steel. Ceram Int. 2008;34(5):1303–7. doi:10.1016/j.ceramint.2007.03.002.
9. Yang BC, Uchida M, Kim HM, Zhang XD, Kokubo T. Preparation of bioactive titanium metal via anodic oxidation treatment. Biomaterials. 2004;25(6):1003–10. doi:10.1016/S0142-9612(03)00626-4.
10. Cabrini RL, Guglielmotti MB, Almagro JC. Histomorphometry of initial bone healing around zirconium implants in rats. Implant Dent. 1993;2(4):264–7.
11. Saldaña L, Méndez-Vilas A, Jiang L, Multigner M, González-Carrasco JL, Pérez-Prado MT, et al. In vitro biocompatibility of an ultrafine grained zirconium. Biomaterials. 2007;28(30):4343–54. doi:10.1016/j.biomaterials.2007.06.015.
12. Wang K. The use of titanium for medical applications in the USA. Mat Sci Eng A. 1996;213(1–2):134–7. doi:10.1016/0921-5093(96)10243-4.
13. Scarano A, Piattelli M, Caputi S, Favero GA, Piattelli A. Bacterial adhesion on commercially pure titanium and zirconium oxide disks: an in vivo human study. J Periodontol. 2004;75(2):292–6. doi:10.1902/jop.2004.75.2.292.
14. Gomez Sanchez A, Schreiner W, Duffó G, Ceré S. Surface modification of titanium by anodic oxidation in phosphoric acid at low potentials. Part 1. Structure, electronic properties and thickness of the anodic films. Surf Interface Anal. 2013;45(6):1037–46. doi:10.1002/sia.5210.
15. Gomez Sanchez A, Ballarre J, Orellano JC, Duffó G, Ceré S. Surface modification of zirconium by anodisation as material for permanent implants: in vitro and in vivo study. J Mater Sci. 2012;. doi:10.1007/s10856-012-4770-8.
16. Gomez Sanchez A, Schreiner W, Duffó G, Ceré S. Surface characterization of anodized zirconium for biomedical applications.

Appl Surf Sci. 2011;257(15):6397–405. doi:10.1016/j.apsusc.2011.02.005.
17. Ballarre J, Seltzer R, Mendoza E, Orellano JC, Mai YW, Garcia C, et al. Morphologic and nanomechanical characterization of bone tissue growth around bioactive sol-gel coatings containing wollastonite particles applied on stainless steel implants. Mat Sci Eng C. 2011;31(3):545–52. doi:10.1016/j.msec.2010.11.030.
18. Sul YT, Johansson CB, Jeong Y, Albrektsson T. The electrochemical oxide growth behaviour on titanium in acid and alkaline electrolytes. Med Eng Phys. 2001;23(5):329–46. doi:10.1016/S1350-4533(01)00050-9.
19. Ballarre J, Manjubala I, Schreiner WH, Orellano JC, Fratzl P, Cere S. Improving the osteointegration and bone-implant interface by incorporation of bioactive particles in sol-gel coatings of stainless steel implants. Acta Biomater. 2010;6(4):1601–9. doi:10.1016/j.actbio.2009.10.015.
20. Perez CA, Radtke M, Sanchez HJ, Tolentino H, Neuenshwander RT, Barg W, et al. Synchrotron radiation X-ray fluorescence at the LNLS: beamline instrumentation and experiments. X-Ray Spectrom. 1999;28(5):320–6. doi:10.1002/(SICI)1097-4539(199909/10)28:5<320:AID-XRS359>3.0.CO;2-1.
21. Sole VA, Papillon E, Cotte M, Walter P, Susini J. A multiplatform code for the analysis of energy-dispersive X-ray fluorescence spectra. Spectrochim Acta B. 2007;62(1):63–8. doi:10.1016/j.sab.2006.12.002.
22. Rinnerthaler S, Roschger P, Jakob HF, Nader A, Klaushofer K, Fratzl P. Scanning small angle X-ray scattering analysis of human bone sections. Calcif Tissue Int. 1999;64(5):422–9. doi:10.1007/PI00005824.
23. Roschger P, Gupta HS, Berzanovich A, Ittner G, Dempster DW, Fratzl P, et al. Constant mineralization density distribution in cancellous human bone. Bone. 2003;32(3):316–23. doi:10.1016/S8756-3282(02)00973-0.
24. Gamsjaeger S, Masic A, Roschger P, Kazanci M, Dunlop JWC, Klaushofer K, et al. Cortical bone composition and orientation as a function of animal and tissue age in mice by Raman spectroscopy. Bone. 2010;47(2):392–9. doi:10.1016/j.bone.2010.04.608.
25. Yerramshetty JS, Akkus O. The associations between mineral crystallinity and the mechanical properties of human cortical bone. Bone. 2008;42(3):476–82. doi:10.1016/j.bon.2007.12.001.
26. Penel G, Leroy G, Rey C, Bres E. MicroRaman spectral study of the PO_4 and CO_3 vibrational modes in synthetic and biological apatites. Calcif Tissue Int. 1998;63(6):475–81. doi:10.1007/s002239900561.
27. Donnelly E, Boskey AL, Baker SP, van der Meulen MCH. Effects of tissue age on bone tissue material composition and nanomechanical properties in the rat cortex. J Biomed Mater Res A. 2010;92A(3):1048–56. doi:10.1002/Jbm.A.32442.
28. Mendonça G, Mendonça DBS, Aragão FJL, Cooper LF. Advancing dental implant surface technology: from micron- to nanotopography. Biomaterials. 2008;29(28):3822–35. doi:10.1016/j.biomaterials.2008.05.012.
29. Sul YT, Kang BS, Johansson C, Um HS, Park CJ, Albrektsson T. The roles of surface chemistry and topography in the strength and rate of osseointegration of titanium implants in bone. J Biomed Mater Res A. 2009;89A(4):942–50. doi:10.1002/jbm.a.32041.
30. Sul YT. The significance of the surface properties of oxidized titanium to the bone response: special emphasis on potential biochemical bonding of oxidized titanium implant. Biomaterials. 2003;24(22):3893–907. doi:10.1016/S0142-9612(03)00261-8.
31. Hanawa T. In vivo metallic biomaterials and surface modification. Mat Sci Eng A. 1999;267(2):260–6. doi:10.1016/S0921-5093(99)00101-X.
32. Cipriano CA, Issack PS, Beksac B, Della Valle AG, Sculco TP, Salvati EA. Metallosis after metal-on-polyethylene total hip arthroplasty. Am J Orthop. 2008;37(2):E18–25.
33. Kerschnitzki M, Wagermaier W, Liu YF, Roschger P, Duda GN, Fratzl P. Poorly ordered bone as an endogenous scaffold for the deposition of highly oriented lamellar tissue in rapidly growing ovine bone. Cells Tissues Organs. 2011;194(2–4):119–23. doi:10.1159/000324467.
34. Liu YF, Manjubala I, Schell H, Epari DR, Roschger P, Duda GN, et al. Size and habit of mineral particles in bone and mineralized callus during bone healing in sheep. J Bone Miner Res. 2010;25(9):2029–38. doi:10.1002/Jbmr.84.
35. Guglielmotti MB, Guerrero C, Cabrini RL. Chronodynamic evaluation of the stages of osseointegration in zirconium laminar implants. Acta Odontol Latinoam. 1997;10(1):11–23.
36. Cipitria A, Lange C, Schell H, Wagermaier W, Reichert JC, Hutmacher DW, et al. Porous scaffold architecture guides tissue formation. J Bone Miner Res. 2012;27(6):1275–88.